

Dynamical low-energy electron-diffraction analysis of bismuth and antimony epitaxy on GaAs(110)

W. K. Ford* and T. Guo†

Advanced Materials Center and Department of Physics, Montana State University, Bozeman, Montana 59717

D. L. Lessor

Pacific Northwest Laboratory, Richland, Washington 99352

C. B. Duke

Xerox Webster Research Center, 800 Phillips Road, 0114-38D Webster, New York 14580

(Received 14 June 1990)

The atomic geometry of Bi adsorbed on GaAs(110) is determined using low-energy electron diffraction (LEED) and compared with calculated atomic geometries of GaAs(111)- $p(1 \times 1)$ -Sb and clean GaAs(110). The analysis of the one-monolayer, epitaxial films is facilitated by comparing LEED intensity data measured for each system under identical experimental conditions and analyzed using a common multiple-scattering model. The overlapping chain geometry, recently proposed as a possible alternative to the previously determined geometry for the GaAs(110)- $p(1 \times 1)$ -Sb system, was tested for both the Sb and Bi systems. Comprehensive multiple-scattering calculations indicate, however, that the previously determined geometry provides the superior fit to the LEED intensity measurements. Several improvements to the LEED analysis methodology, including simultaneous multidimensional optimization, are described.

I. INTRODUCTION

Antimony and bismuth form ordered monolayers on a wide range of different III-V (110) surfaces. Hence, these epitaxial V/III-V (110) systems constitute useful prototypes for investigations of issues related to surface chemical bonding, electronic structure, and growth because their two-dimensional order enables detailed experimental and theoretical studies to be performed. A first step to any comprehensive investigation of epitaxy using these prototype systems is the determination of their surface atomic geometries. The most widely studied V/III-V (110) system is that of GaAs(110)- $p(1 \times 1)$ -Sb. The accepted geometry, depicted in Fig. 1, was proposed heuristically by Goddard¹ and established experimentally using low-energy electron diffraction (LEED).² The Goddard geometry has subsequently been confirmed using scanning tunneling microscopy (STM) (Ref. 3) and indirect methods, such as high-resolution core-level spectroscopy.⁴

Recently, however, several alternate geometric models have been proposed on the basis of total-energy minimization calculations using a tight-binding Hamiltonian.⁵ One of these structures, which we term the relaxed Skeath model or the overlapping-chain model, not only forms a stable geometry energetically equivalent to the Goddard model within the tight-binding approximation but also provides an equally satisfactory interpretation of the STM micrographs.^{3,5} The relaxed Skeath geometry is depicted in Fig. 2. Although the initial LEED investigation of GaAs(110)- $p(1 \times 1)$ -Sb considered one form of the Skeath chain geometry and rejected it as failing to describe the observed intensities, those calculations did not consider the impact of modifications of the substrate

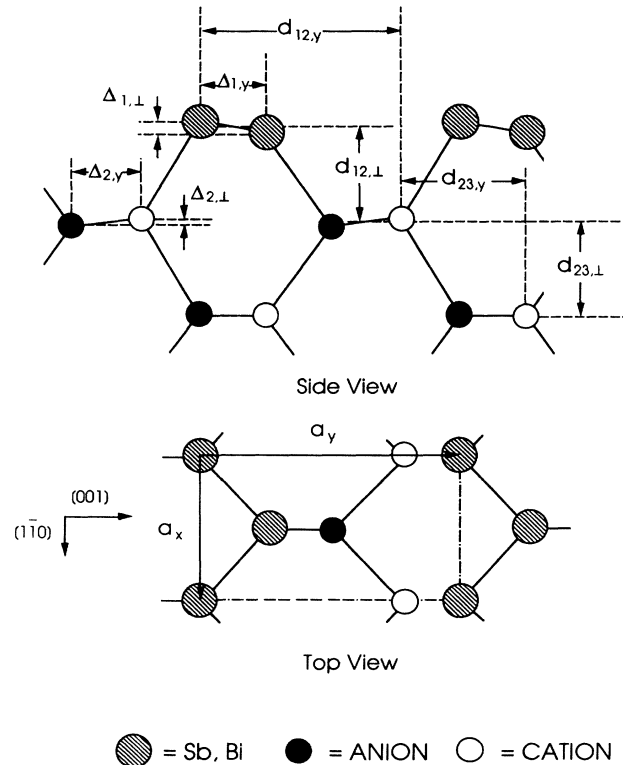


FIG. 1. Schematic drawing of the Goddard structural and model depicting Sb or Bi bonded to a zinc-blende (110) substrate. The first- and second-layer shear angles are given as $\omega_i = \arctan(\Delta_{i,l} / \Delta_{i,y})$ for $i=1,2$. A negative ω_1 and a positive ω_2 are depicted in the drawing.

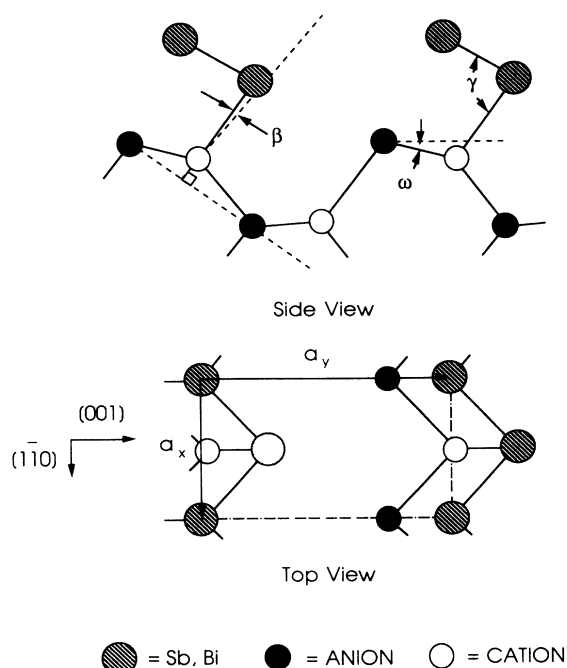


FIG. 2. Schematic drawing of the Skeath structural model depicting Sb or Bi bonded to a zinc-blende (110) substrate. β is positive, ω is negative, and $\gamma \approx \pi/2$, as depicted in the drawing.

bonding. The tight-binding calculations have established, however, that a modification of the clean surface geometry is an important aspect of the minimum energy structure, and suggest that the LEED analysis should be extended to include this effect.

Like the STM studies, analysis of angle-resolved photoemission data has not been able to differentiate between the two models.⁵ The surface-state wave functions calculated for the Goddard and Skeath geometries embody significant differences in the electronic structure corresponding to the two geometries.⁵ In the Goddard model⁶ a band of p^2 states is formed, extending along the $[1\bar{1}0]$, zig-zag chain direction, cf. Fig. 1. A second band of Sb $p_z\pi$ states hybridize with the substrate sp^3 dangling bonds to bond the overlayer to the substrate. Whereas the p^2 states are localized within the zig-zag chain, they do not mix significantly with the substrate dangling-bond orbitals. However, the Sb π energy bands are predicted to split due to the interaction with the substrate states and to form four surface-state bands.⁶ The electronic structure of the relaxed Skeath geometry is entirely different.⁵ The Sb atomic orbitals possess p^3 character and fail to hybridize into intrachain and overlayer-substrate bands as predicted for the Goddard model. Thus, the qualitative differences between the predicted surface-state electronic structures could, in principle, be used to differentiate between the two geometric models. Nevertheless, the extant measurements of surface bands for this system have proven inadequate to resolve between the predictions of the two-model geometries.

Bismuth adsorption to III-V(110) surfaces has drawn considerable recent attention.⁷⁻¹⁵ Being isoelectronic

with Sb, Bi might be expected to have bonding properties analogous to Sb. However, we have recently reported that unlike Sb, Bi displays richly varying ordering properties on the III-V(110) surfaces.⁷ Furthermore, although Bi and Sb form similar bonds in small molecules¹⁶ they bond very differently in network solids: Sb is a semimetal as a monatomic element but forms tetrahedrally coordinated compound semiconductors, such as InSb and GaSb; Bi is also a semimetal as an elemental material but forms p^3 coordinated materials, such as InBi which has a PbO structure.¹⁷ Hence, Bi is a more likely candidate than Sb to exhibit a p^3 chain geometry on the III-V (110) surfaces. If differences in the surface atomic geometry of these two adsorbates exist, they could also be manifested as differences in the chemical and electrical properties of the two overlayers.

The discovery that bismuth exceeds antimony in forming interesting epitaxial films on III-V(110) surfaces,⁷ the results of the total-energy calculations reported for antimony epitaxy,⁵ and the difficulty of distinguishing between the two candidate geometric models described above motivate the present study of the geometry of column V adsorbates on zinc-blende (110) surfaces. We present a systematic study of the geometry of Sb and Bi monolayers on GaAs(110) using LEED multiple-scattering analysis. LEED intensity (IV) data for GaAs(110), Sb/GaAs(110), and Bi/GaAs(110) have been measured in the same experimental chamber and have been analyzed using a common theoretical model. In this fashion, a self-consistent description of the surface geometry of these three systems has been developed.

II. EXPERIMENTAL TECHNIQUE

The experiments were performed in an ultrahigh-vacuum chamber with a base pressure of less than 1×10^{-10} Torr. The chamber was equipped with standard LEED optics, a sample cleaver, and two evaporation sources. The GaAs crystals were cut into 5 mm square bars oriented to within 0.5° along the $[110]$ direction. Using a diamond saw notches 0.040 in. deep and 0.020 in. wide were cut into the side of each bar at 0.085 in. intervals to assist in the cleaving process. A button heater was attached to the sampler holder near the base of the crystal and three thick copper braids were used to connect the sample holder to a liquid-nitrogen reservoir. This design allowed the samples to be cooled to 120 K and heated in excess of 500°C .

Bi and Sb films were deposited onto the freshly cleaved substrates by sublimation from high-purity (99.9999%) polycrystalline material held in shielded tungsten wire baskets. The sublimation temperature was approximately 480°C for Bi and somewhat less for Sb. The two sources were simultaneously available but were physically isolated to eliminate cross contamination of the sources. Slow deposition rates were used, typically less than $1 \text{ \AA}/\text{min}$ as monitored using a quartz-crystal oscillator thin-film monitor (QCO). The QCO was calibrated by calculation and by direct comparisons to core-level photoemission results.¹³ In a few cases, the samples were transferred for calibration from the experimental chamber to a Ruther-

ford backscattering facility where it was determined that the QCO calibration can be relied upon to within approximately 10%.¹¹ The depositions were performed at room temperature. No differences were observed between the LEED IV curves measured for Sb or Bi films prepared at room temperature and those for the corresponding annealed films. In the Sb/GaAs(110) case, changes in the electronic structure due to annealing were observed previously using photoemission and interpreted as improvements in the structural order of the Sb overlayer.⁴ Our LEED measurements indicate that the effect of annealing on the structure of the Sb/GaAs system is short ranged and too subtle to impact our IV studies.

Leed and Auger spectroscopy, via the retarding field analyzer method, were performed using a video LEED instrument described previously.¹⁸ The ordered films studied each displayed the $(\bar{h}k)=(hk)$ symmetry of the cleaved III-V (110) surfaces, where the beam index convention is that common in the literature.^{19,20} All data were taken at normal incidence. The LEED alignment procedure, which matches the intensity curves of the $(\bar{h}k)=(hk)$ symmetry-equivalent beams, has been described in our previous work.¹⁸ After alignment the samples were cooled to below 150 K before the final IV data sets were measured. A typical set of IV curves was measured in 2-eV steps from 50 to 300 eV incident energy in less than 5 min. Although the diffraction intensities were collected two or three times for each film prepared, no beam-induced surface degradation occurred because of the short-data collection times permitted by our instrument. Prior to analysis, corresponding data sets were averaged and normalized to the incident beam current, which varies with beam energy in the LEED apparatus used.¹⁸ In addition to the IV data, entire diffraction patterns were integrated, digitized, and stored within the computer to provide a semiquantitative measure of surface quality.

The reproducibility of the experimental data is important to any surface geometry determination. Accordingly, several tests were conducted that allow us to improve our estimate of reproducibility relative to that quoted previously.¹⁸ The x-ray reliability factor R_x is the figure of merit used in the calculations discussed below to compare the calculated and experimental IV data sets.²¹ It, thus, provides a relevant measure with which to judge the reproducibility of the experiments. Several sets of data were collected using different, freshly cleaved clean GaAs(110) surfaces. We found that R_x variations of 0.01 typically occur between scans containing 14 beams over a 50 to 300 eV energy range from different cleaves. Figure 3 shows, for example, the six strongest beams of two independent measurements from different cleaves. Statistical fluctuations can be reduced if data from two or more repeated sets of measurements are averaged. We found that the R_x value between IV scans of the same surface is typically 0.001. Therefore, the R_x value of 0.01 quoted above between identical samples is the result of errors in sample alignment and positioning and not due to statistical variations in the data. Finally, after several sets of data are collected they are averaged and normalized to the beam current prior to the multiple-scattering

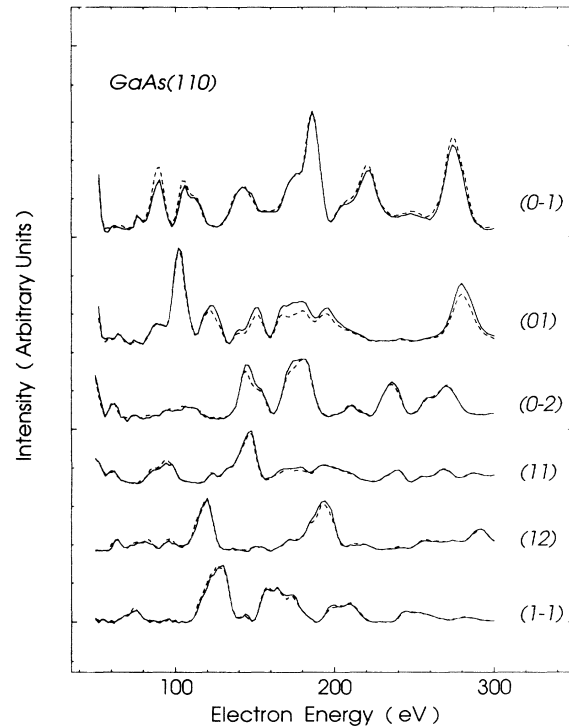


FIG. 3. Intensity of the six strongest diffraction beams taken as a function of electron energy for two different cleaves of GaAs(110) to demonstrate the reproducibility of the IV data. The relative intensities of the beams are retained.

analysis. We computed R_x between individual data sets and the averaged data to estimate the width of the R_x distribution. R_x values of 0.002 were typically obtained which indicate a very narrow distribution in R_x due to experimental conditions.

In previous LEED studies of, e.g., GaAs(110),²² the analyses were performed using different numbers of diffraction beams and different energy ranges than those utilized here. The sensitivity of R_x to the differences in these factors should be considered prior to making a direct comparison of values. A calculation of R_x between our best fit GaAs(110) structure and our experimental data set was performed as a function of the number of beams used in the comparison. Additional beams were included in order of decreasing integrated intensity. The result was that an R_x value very close to the 18 beam value was obtained using only the five strongest beams, and the change in R_x from the 14 beam case to the 18 beam case was less than 0.01. The sensitivity of R_x to the energy range used in the calculation was greater. A comparison of the computed IV data to the experimental data was made for energy ranges from 50 to 200 eV up to 50 to 300 eV. R_x was observed to have considerable fluctuations. The minimum R_x value, 0.17, was obtained for the 50–250 eV range while the maximum value, 0.20, was obtained for the 50–300 eV range. Otherwise, no trends were observed.

III. THEORETICAL METHOD

A. Multiple-scattering model

The LEED IV data was analyzed using the method of Duke and Laramore.²³ This dynamical, multiple-scattering LEED theory is a generalization of the work of Beeby²⁴ in which the complex-valued electron self-energy has been included.²⁵ The success of this theoretical method for atomic geometry determination of semiconductor surfaces has been established for a wide variety of systems similar to the ones discussed herein, making the method a suitable choice to use for our studies.¹⁹ We summarize below the features of the method salient to our present study.

Electron scattering by surface atoms is described using energy-dependent phase shifts. Each atomic scattering center is represented as a neutral atom whose potential is first computed using a relativistic, self-consistent Hartree-Fock-Slater muffin-tin model.²⁶ For the gallium and arsenic cases, the charge densities are modified by superimposing the charge densities of the neighboring sixteen shells of atoms, assuming bulk coordination. The adsorbate atoms, bismuth and gallium, are treated as free atoms and no superpositioning of neighboring charge densities is performed. The Slater $\rho^{1/3}$ exchange term of the computed self-consistent atomic potential is replaced by an energy-dependent Hara exchange term. The Hara exchange model has been established to describe better the physics of electron scattering in LEED, where an external electron with energies greater than 10 eV above than the Fermi level interact with the electron gas at the surface.^{26,27} Finally, the resulting effective-scattering potential is inserted into the radial Schrödinger equation, which is integrated to yield the scattered wave phase shifts. Because the sample temperature at which the data is collected, ~ 150 K, is well below the Debye temperature of bulk GaAs, 345 K, no modeling of temperature effects is included.

The energy-dependent phase shifts obtained from the potential model described above and used in the calculations presented in this paper are plotted for each atom in Fig. 4. The corresponding total elastic cross sections computed using the phase shifts of Fig. 4 are presented in Fig. 5. It is important not to include more phase shifts in the calculation than necessary because the cost of the multiple-scattering calculation increases dramatically with the number of phase shifts used. Although fewer than six phase shifts could be used for the clean surface case, the antimony and bismuth adsorbates are stronger scatterers and, therefore, require a greater number of phase shifts to describe their cross sections adequately. Because the results of trial multiple-scattering calculations using seven phase shifts differed little from those using six phase shifts and because our current computer algorithm requires that the same number of phase shifts be used for each atom we selected to use six phase shifts for all calculations.

In the multiple-scattering calculation, the semi-infinite crystal is replaced by a slab of twelve bilayers (24 atomic layers). An exact calculation of the scattering amplitudes

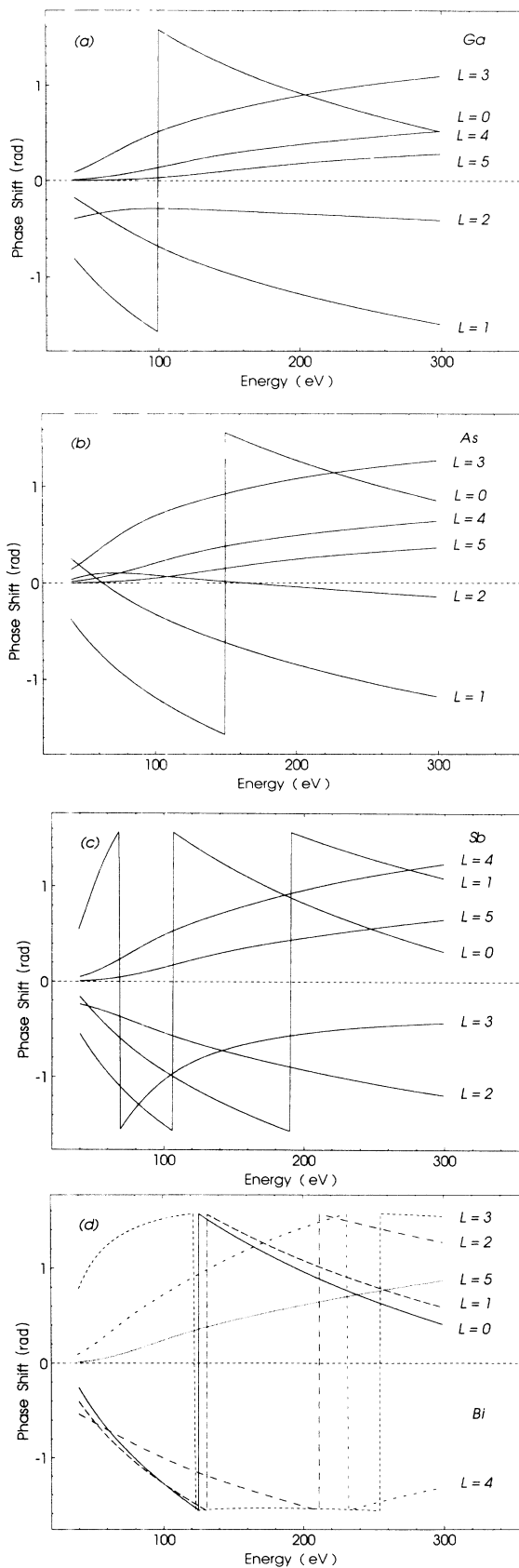


FIG. 4. Energy-dependent phase shifts used in the theoretical calculations: (a) gallium; (b) arsenic; (c) antimony; (d) bismuth. The relativistic Hartree-Fock-Slater crystal potential model with Hara exchange is used.

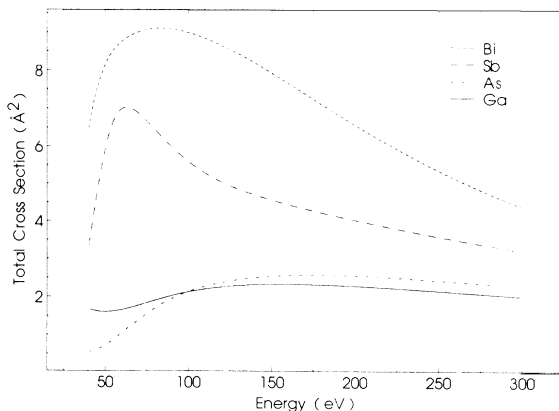


FIG. 5. Total elastic cross sections of gallium, arsenic, antimony, and bismuth computed from the phase shifts shown in Fig. 4 and plotted as a function of incident beam energy.

is performed for the topmost four bilayers, called the surface slab. The exact scattering amplitudes for each of the next eight bilayers are computed individually and added to the amplitudes from the surface slab. The multiple-scattering contributions between the eight underlying bilayers and between those bilayers and the surface slab are not computed. This approximation is justified due to the short elastic mean-free path of the electrons in the energy range of LEED and because the trial geometries considered are constrained to differ from the bulk geometry only in the top two bilayers. This approach has been used successfully in many previous studies of zinc-blende (110) surface structure.¹⁹

B. Method extensions

Several significant extensions to our previous analysis methods have been introduced. The first is the incorporation of the lattice symmetry into the calculations. The intra-plane and inter-plane propagators require the calculation of two-dimensional lattice sums,²⁴ which have been streamlined by performing symmetry adapted summations. In practice this feature has allowed us to reduce the number of distinct unit cells used in the two-dimensional summations to 25 or less from 256 or more, with a concomitant savings in computer cost.

The second extension is the automation of the structure search process using the simplex method. With this method the structural and nonstructural parameters are adjusted in a nonlocal search for the best fit between the calculated and measured IV curves. R_x is the figure of merit used for our searches. An alternate figure of merit, the weak integrated distance reliability factor,²⁸ was also tried in some of the calculations. The predicted geometries did not differ significantly, however, from those obtained using R_x in the cases examined. The simplex method begins with a given set, or simplex, of trial values, or vertices, for each calculational parameter and systematically excludes the worst values until a convergence criterion is satisfied. Upon iteration of the simplex

algorithm the spread in values of each parameter is reduced. The method and its advantages and disadvantages are discussed elsewhere.²⁹ In our experience a seven parameter search converges within approximately thirty simplex steps.

There are seven adjustable parameters in the geometric models discussed below: five structural ones consisting of bond lengths and bond angles, cf. Figs. 1 and 2, and two nonstructural ones corresponding to the real and imaginary parts of the electron self-energy. In our previous studies a self-energy model having a constant inelastic collision mean-free path, λ_{ee} , was selected.²² A new choice of self-energy model, in which λ_{ee} is energy dependent, is made here because the data is collected over a wider energy range so that the choice of a constant λ_{ee} is not justified. A second difference from our previous approaches is that previously the real part of the inner potential, V_0 , was fitted by adjusting the final computed IV curves by a fixed energy amount. In the calculations presented below V_0 is treated on an equal footing with the other parameters of the model and no rigid shift of the energy scale is subsequently performed.

In our experience searches initiated using all seven parameters usually resulted in physically implausible bond lengths. This tendency is related to the interplay between V_0 , the effective index of refraction, and the interlayer spacing. Therefore, a two-step search procedure was developed based on the concept that bond rotations are the most important factor in determining geometry. In the first step the search is performed keeping the bond lengths fixed. In the case of Ga-As the nearest-neighbor distance found in the bulk, 2.45 Å, was selected; in other cases the sum of the covalent radii was used. The remaining set of five parameters are selected over reasonable ranges of parameter values to form the eight initial vertices of the simplex. The search is begun and stopped when the spread in all remaining parameters is judged sufficiently small. Typically, the figure of merit, R_x converges more quickly than do the individual fit parameters. In the second step, a new simplex is constructed about the previous best vertex, the one having the smallest R_x . Seven new vertices are selected using the same condition stated above, that a reasonable range of parameters be included in the simplex. However, in the second step the bond lengths are also allowed to vary by 10–20% of their covalent values. If desirable, after convergence of the second step, a new simplex centered on the best vertex of the previous search is prepared and a third search conducted. In each case where a small R_x value (~ 0.25) was obtained, however, a third search reproduced the previously obtained geometry, serving to increase our confidence that the R_x minimum attained was a global minimum.

At completion of the simplex searches, additional calculations are performed to refine the results and to provide a measure of how sensitive the minimum is to variations in individual parameters. Each parameter is varied individually keeping the other parameters fixed at the simplex-optimized values. These additional calculations are desirable due to the slow convergence the simplex method displays when it is near a minimum.²⁹ In all

cases considered the refined values obtained were very close to those determined that resulted at the end of the simplex search.

It is well known that in general for zinc-blende (110) surfaces R_x generally exhibits many local minima.¹⁹ Care must be taken, therefore, to ensure that a physically reasonable but wide range of parameter values is used to initiate each simplex search or misleading conclusions may be reached. An example of the occurrence of multiple local minima is presented in Fig. 6 where R_x is plotted versus the top layer shear angle for GaAs(110) while fixing the other parameters at their best fit values, cf. Table I. The oscillations in R_x occur because variations in ω_1 modify the relative positions of two atomic planes and, therefore, the phase relationships of the diffracting electrons, cf. Fig. 1. In Fig. 6 several distinct minima in the range of ω_1 plotted can be seen. Nevertheless, it is our experience that using either R_x or the weak integrated distance reliability factor the simplex method leads to only one best fit value when the geometric model is correct. Therefore, Fig. 6 demonstrates the adequacy of the LEED theory and the R_x search method to unambiguously determine a correct geometric structure.

To accommodate the changes described above a new dynamical LEED computer code has been written at Montana State University. The current code incorporates our extensions and can be run efficiently on either the Cray XMP at the National Center for Supercomputing Applications or our university VAX 8550 with few modifications. The software used in previous studies¹⁹ was optimized for the CDC 205 and could not easily be transported to other computer architectures. The present code performs a typical calculation using six phase shifts and four exact bilayers in 1.2 sec per energy point on the Cray YMP.

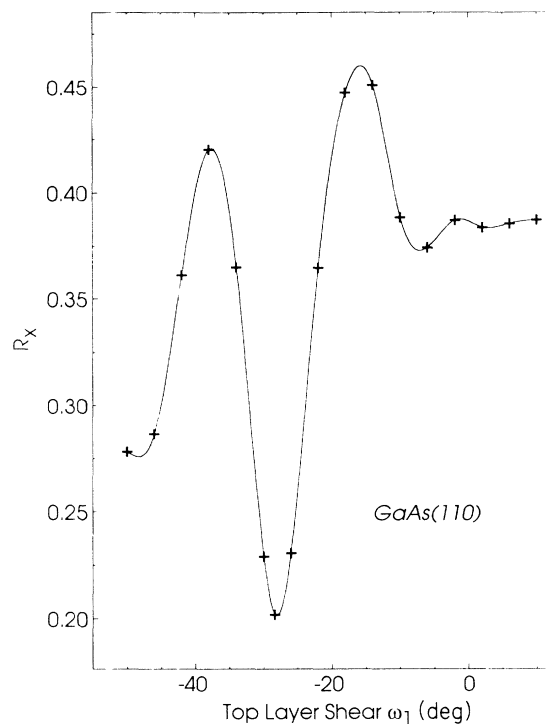


FIG. 6. Variation of R_x with the top-layer shear angle, ω_1 , for the best fit structure for clean GaAs(110). The other model parameters used are those listed in Table I.

IV. RESULTS

A. GaAs(110)

The intensities of eighteen inequivalent diffraction beams from clean GaAs(110) were measured over an

TABLE I. Results of the dynamical LEED analysis using the Goddard structural model, cf. Fig. 1. C_i-A_j corresponds to the bond length between the atom in the cation position of layer i and the atom in the anion position of layer j . V_0 and V_1 refer to the real and imaginary parts of the inner potential.

| Goddard model | ω_1 (deg) | C_2-A_1 (Å) | C_1-A_1 (Å) | C_1-A_2 (Å) | ω_2 (deg) | V_0 (eV) | V_1 (eV) | R_x |
|-------------------|------------------|---------------|---------------|---------------|------------------|------------|------------|-------|
| GaAs(110) | | | | | | | | |
| Fixed bond length | -30.0 | 2.45 | 2.45 | 2.45 | 3.2 | 13.0 | 3.4 | 0.223 |
| Best fit | -28.4 | 2.42 | 2.48 | 2.38 | 3.4 | 12.4 | 3.8 | 0.204 |
| Sb/GaAs | | | | | | | | |
| Fixed bond length | -2.5 | 2.66 | 2.80 | 2.60 | 3.3 | 10.3 | 3.2 | 0.204 |
| Best fit | -2.3 | 2.64 | 2.77 | 2.66 | 4.5 | 10.4 | 3.5 | 0.199 |
| Bi/GaAs | | | | | | | | |
| Fixed bond length | -4.3 | 2.72 | 2.92 | 2.66 | 3.2 | 9.8 | 2.7 | 0.263 |
| Best fit | -2.6 | 2.73 | 2.87 | 2.77 | 4.3 | 10.2 | 3.4 | 0.238 |

overall energy range of 50–300 eV. The IV data are presented in Fig. 7, grouped according to integrated intensity with no correction for variation in the energy range of each beam. In order of decreasing intensities the beams are $0\bar{1}$, 01 , $0\bar{2}$, $11 = \bar{1}1$, $12 = \bar{1}2$, $1\bar{1} = \bar{1}\bar{1}$, $10 = \bar{1}0$, 02 , 03 , $2\bar{1} = \bar{2}1$, $1\bar{2} = \bar{1}2$, $20 = \bar{2}0$, $1\bar{3} = \bar{1}3$, $13 = \bar{1}\bar{3}$, $0\bar{3}$, $21 = \bar{2}1$, $2\bar{2} = \bar{2}2$, and $22 = \bar{2}2$. Within each panel in Fig. 7 the rela-

tive intensities of the beams are maintained.

Due to the extensive previous studies of the atomic geometry of GaAs(110) (Ref. 30) only the rotational relaxation model, cf. Fig. 1, was used in the IV analysis. Five structural parameters were considered: the first- and second-layer shear angles, ω_1 and ω_2 , and the bond lengths of the gallium and arsenic atoms in the top layer

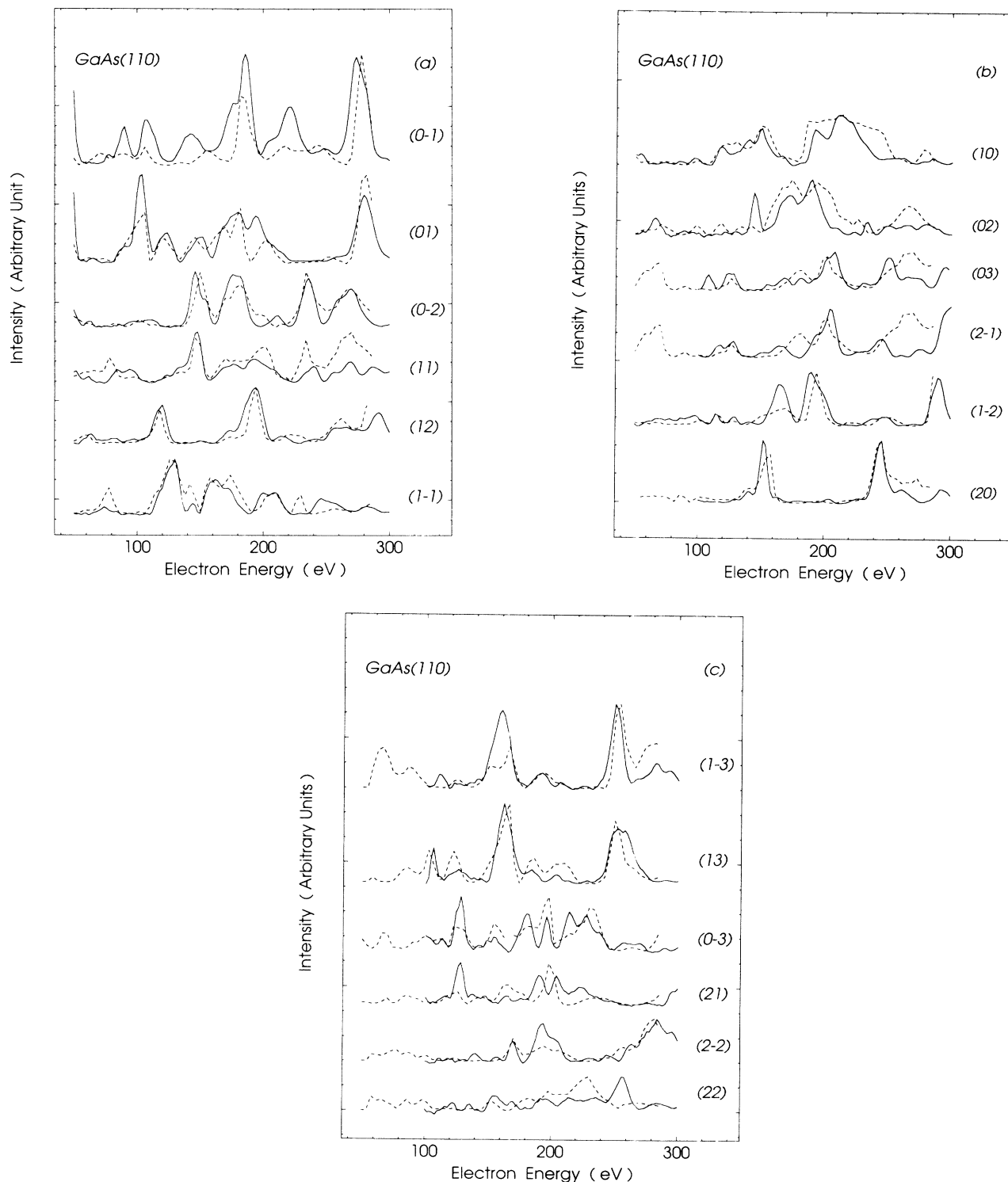


FIG. 7. Clean GaAs(110) IV data, solid curves, grouped according to integrated beam intensities. The relative intensities of the beams are retained within each panel. The dashed lines are the computed intensities of the best fit structural model listed in Table I.

and between the first and second layers. In terms of the parameters listed in Fig. 1, the shear angles ω_i are given by $\arctan(\Delta_{i,1}/\Delta_{i,y})$ for $i=1,2$ with a counter-clockwise rotation from horizontal being positive.

Table I lists the structure we have determined for GaAs(110) using the search method described above and the structural parameters indicated in Fig. 1. Two sets of results are listed for GaAs(110). The first was obtained by performing a five parameter simplex search in which the bond lengths were fixed at the bulk nearest-neighbor distance, 2.45 Å. The second was obtained after a seven parameter search was performed about the first, five parameter result. The best fit geometry listed was refined from the results of the final simplex search in the manner described above. Only 30 iterations were used in each simplex search. Except for V_0 , the parameters listed in Table I are at the bottom of a symmetric minimum in R_x . The minimum in V_0 is, however, very broad and irregular. This irregularity occurred, in part, because changes in the value of V_0 can change the range of kinetic energies that exit the crystal for each diffracted beam and, in turn, modify the energy range over which R_x is computed.

B. Sb/GaAs(110)

The averaged and normalized IV data for the GaAs(110)- $p(1 \times 1)$ -Sb system are plotted in Fig. 8. The eighteen beams used in the structure determination are $01, 0\bar{1}, 0\bar{2}, 11=\bar{1}\bar{1}, 1\bar{1}=\bar{1}\bar{1}, 12=\bar{1}\bar{2}, 1\bar{2}=\bar{1}\bar{2}, 10=\bar{1}\bar{0}, 02, 03, 20=\bar{2}\bar{0}, 13=\bar{1}\bar{3}, 0\bar{3}, 2\bar{1}=\bar{2}\bar{1}, 13=\bar{1}\bar{3}, 22=\bar{2}\bar{2}, 2\bar{2}=\bar{2}\bar{2},$ and $21=\bar{2}\bar{1}$, listed in order of decreasing integrated intensities on the energy range of 50 to 300 eV.

Three classes of geometries were considered in the calculations: Goddard, disordered, and Skeath. The Goddard model is depicted in Fig. 1. This model is the accepted geometry for Sb/GaAs(110) and has been supported by the results of LEED (Ref. 2) and STM (Ref. 3) studies. The results of the new calculations using our present analysis method serve to confirm the results of the previous LEED analysis² and provide a consistent reference for the bismuth calculations presented in this paper. The geometric parameters determined in our two-step search are listed in Table I. The calculated IV curves for the best fit geometry are plotted against the experimental

data in Fig. 8. The quality of the fit, measured using either visual comparison or R_x , is consistent with that obtained for GaAs(110) in Fig. 7.

The second geometric model considered was the disordered model. STM has established that at one-monolayer coverage both antimony and bismuth order on GaAs(110).³ This conclusion cannot be made directly using LEED IV data because electron scattering involves the top several atomic layers of the surface. The effect of a disordered overlayer is to increase the background intensity in the LEED pattern. The background is subtracted, however, from the IV curves during measurement and so, information regarding the order of the overlayer is lost. It is also difficult to measure the background intensity directly in an experimentally meaningful way. Nevertheless, an indirect test of order in the overlayer can be made by assuming a disordered geometric model in the multiple-scattering analysis of the IV data. With this approach the IV data of the overlayer system is analyzed using the geometry and phase shifts appropriate for the clean surface and bond angles and the self-energy components are allowed to vary. It is assumed that although the adsorbed Sb atoms may modify the geometry of the top GaAs layer they are arranged without long-range order and, thus, do not directly contribute to the IV data. The diffraction geometry is analogous to that depicted in Fig. 1 with the overlayer atoms replaced by gallium and arsenic.

The disordered model has been tested for the Sb overlayer system, cf. Table II. The best results of two simplex searches for this geometry are listed. The searches differ by the choice of bond lengths made. The first choice retains the bulk nearest-neighbor distance, 2.45 Å. It corresponds to a picture in which the adatoms bond to the substrate without modification of the bond lengths in the substrate periodic lattice. In the second case, the covalent bond lengths of the antimony overlayer system were selected but only gallium and arsenic phase shifts were used in the calculations.

Because the best R_x value found in each case was found to lie outside the range that leads to a convincing fit, i.e., $R_x \geq 0.3$, and because the disordered geometric model is inconsistent with the STM data,³ no further variation of the bond lengths was attempted.

The third geometry tested was the relaxed Skeath mod-

TABLE II. Results of the dynamical LEED analysis using the disordered structural model. The parameters are the same as listed in Table I. The rows labeled 1 are the results of a search fixing the bond lengths at the nearest-neighbor distance of bulk GaAs. The rows labeled 2 are the results of a search fixing the bond lengths at the covalent values listed for the overlayer systems in Table I.

| Disordered model | ω_1 (deg) | C_{2-A_1} (Å) | C_{1-A_1} (Å) | C_{1-A_2} (Å) | ω_2 (deg) | V_0 (eV) | V_1 (eV) | R_x |
|------------------|------------------|-----------------|-----------------|-----------------|------------------|------------|------------|-------|
| Sb/GaAs | | | | | | | | |
| 1 | -35.0 | 2.45 | 2.45 | 2.45 | 1.7 | 10.0 | 3.4 | 0.396 |
| 2 | -12.0 | 2.66 | 2.80 | 2.60 | 4.5 | 7.6 | 3.0 | 0.322 |
| Bi/GaAs | | | | | | | | |
| 1 | -6.4 | 2.45 | 2.45 | 2.45 | -7.4 | 13.0 | 2.4 | 0.384 |
| 2 | -9.8 | 2.72 | 2.92 | 2.66 | 5.0 | 13.5 | 3.4 | 0.358 |

el, cf. Fig. 2. The calculations presented here generalize our previous study² by considering relaxations of the substrate in response to the overlayer bonding. Our results are presented in Table III. In the first step of the search, the intrachain bond length and the overlayer to substrate

cation bond lengths were held to their covalent values as listed in the table. The converged calculation did not attain a satisfactory R_x value. A second search that induced bond-length variations was then performed but also did not yield a satisfactory R_x factor, cf. Table III.

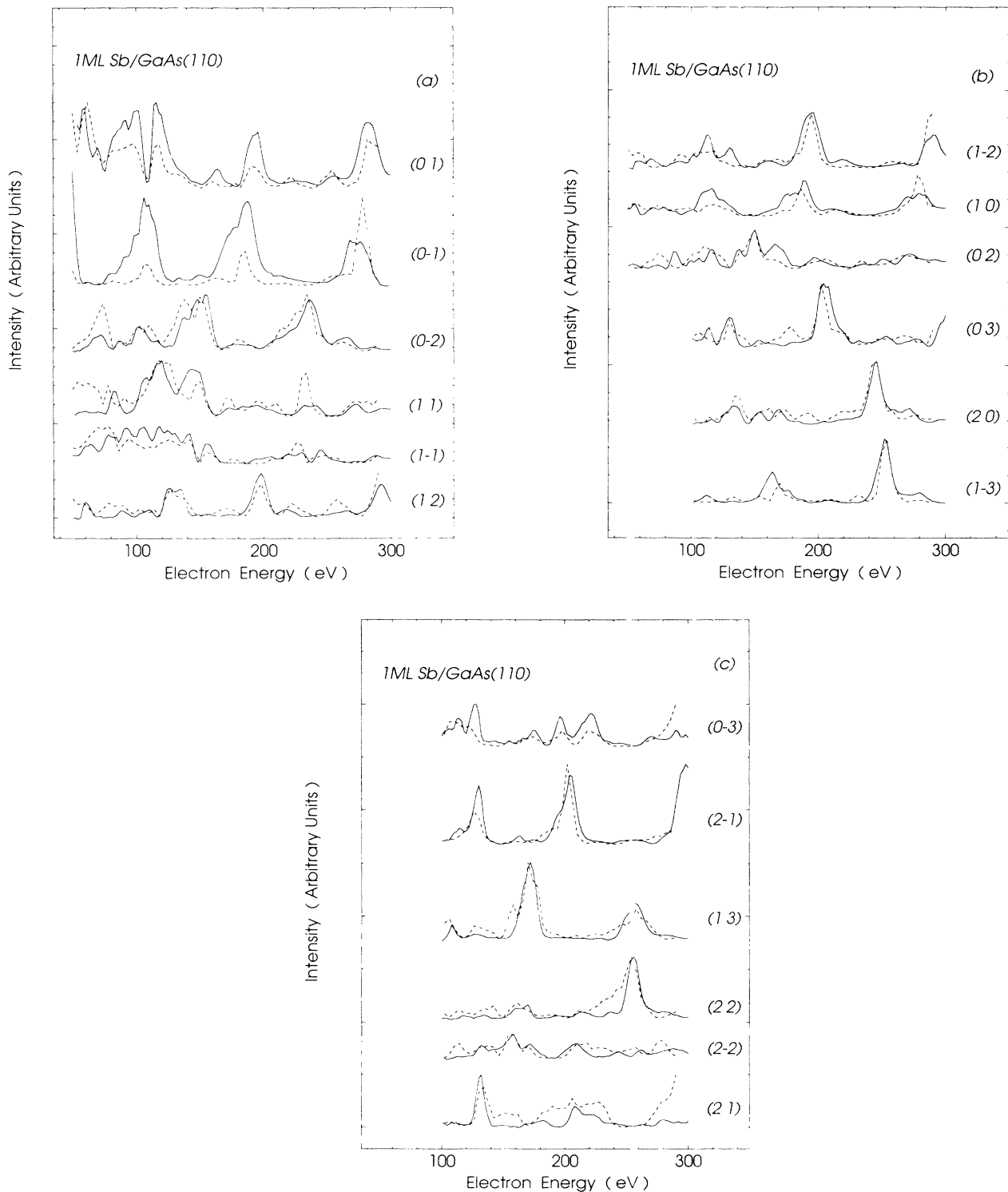


FIG. 8. Sb/GaAs(110) IV data, solid curves, grouped according to integrated beam intensities. The relative intensities of the beams are retained within each panel. The dashed lines are the computed intensities of the best fit structural model listed in Table I.

TABLE III. Results of the dynamical LEED analysis using Skeath structural model, cf. Fig. 2.

| Skeath model | γ (deg) | β (deg) | C_2-A_1 (Å) | C_1-A_1 (Å) | ω_2 (deg) | V_0 (eV) | V_1 (eV) | R_x |
|-------------------|----------------|---------------|---------------|---------------|------------------|------------|------------|-------|
| Sb/GaAs | | | | | | | | |
| Fixed bond length | 50.1 | -4.6 | 2.66 | 2.80 | 2.6 | 10.2 | 4.0 | 0.326 |
| Best fit | 52.5 | -3.7 | 2.63 | 2.75 | 1.7 | 10.1 | 3.9 | 0.322 |
| Bi/GaAs | | | | | | | | |
| Fixed bond length | 35.6 | 1.0 | 2.72 | 2.92 | -1.4 | 11.1 | 3.2 | 0.369 |
| Best fit | 37.4 | 4.0 | 2.69 | 2.92 | -0.9 | 10.1 | 2.8 | 0.341 |

C. Bi/GaAs(110)

The growth characteristics of the Bi/GaAs(110) interface have been reported previously.¹¹ A sixth-order periodicity in the LEED was discovered and interpreted to correspond to the short 10 or 11 atom bismuth chains running along the $[1\bar{1}0]$ direction observed in STM micrographs.¹⁵ The (6×1) periodicity suggests that an exact LEED calculation should employ a (6×1) unit cell. However, the quality of the sixth-order periodicity was very dependent on sample preparation.⁸ Annealing one-monolayer films improved only marginally the quality of the (6×1) LEED pattern, which generally only displayed one fractional order spot on only some of the beams over small energy intervals. Furthermore, the fractional order spots were broader than the integral order ones due to increased surface disorder.⁸ Therefore, it was decided to approximate the system by analyzing only the integral order beams so that the average geometry of the bismuth chains could be determined. To test this approximation data collected on annealed and unannealed samples were compared. The integral order IV curves were essentially identical for the two sets of samples.

The averaged and normalized IV data for the Bi/GaAs(110) system are plotted in Fig. 9. The eighteen beams used in the structure determination are $01, 0\bar{1}, 0\bar{2}, 11 = \bar{1}\bar{1}, 12 = \bar{1}\bar{2}, 1\bar{1} = \bar{1}\bar{1}, 02, 1\bar{2} = \bar{1}\bar{2}, 20 = \bar{2}0, 13 = \bar{1}3, 03, 2\bar{1} = \bar{2}\bar{1}, 13 = \bar{1}3, 22 = \bar{2}\bar{2}, 0\bar{3}, 10 = \bar{1}0, 21 = \bar{2}\bar{1},$ and $2\bar{2} = \bar{2}\bar{2},$ listed in order of decreasing integrated intensities. As above, the relative intensity of the beams within each panel is retained for comparison. The three geometries tested for the Sb/GaAs(110) system were also tested for the Bi/GaAs(110) system and the results are presented in Tables I–III. Simplex searches were performed for each geometry using the approach described above for the Sb/GaAs(110) system. The calculated IV curves for the best fit geometry, listed in Table I, are plotted together with measured intensities in Fig. 9.

V. DISCUSSION

The first quantitative atomic geometry for the GaAs(110) was proposed in 1976.^{31,32} Since then several studies, including the present work, have revisited the

subject with increasing sophistication.³⁰ The best fit structure listed in Table I is the result of the first structure search in which all the structural and nonstructural parameters were optimized simultaneously and over a broad range of values. In the first part of Table IV, the important structural parameters previously obtained for GaAs(110) using the Duke-Laramore-Beeby multiple-scattering LEED theory,^{22,23} using an alternate multiple-scattering LEED formulation,³⁴ and from medium-energy ion scattering data (MEIS) and Monte Carlo simulations³⁵ are compared to the best fit values of Table I. $\Delta_{1,1}$ and $\Delta_{2,1}$ are depicted in Fig. 1; the shear angles ω are defined above; $\delta y(\text{As})$ and $\delta y(\text{Ga})$ are the lateral displacements of the As and Ga atoms in the top layer relative to the bulk positions; and $\delta d_{12,1}$ is the expansion of the top-layer spacing relative to the bulk, defined as the perpendicular distance between the midpoints of the bilayers.

The geometries indicated in Table IV for clean GaAs(110) are very similar in quality and differ only in the detailed numerical values. The results of three different LEED groups and three different experiments are represented. The agreement between the best fit structures derived using LEED is exceptional. The MEIS analysis also agrees well with the LEED analyses. One difference between the MEIS and LEED studies is, however, that in the analysis of the ion scattering data no second-layer relaxation and no bond-length variations were required to fit the data. In the LEED cases, both a small ω_2 and small bond-length variations were deemed necessary to fit the data. Referring to Table I, our best fit structure predicts a 1.1% contraction of the $\text{As}_1\text{-Ga}_2$ bond, a 2.7% contraction of the $\text{Ga}_1\text{-As}_2$ bond, and a 1.3% expansion of the $\text{As}_1\text{-Ga}_1$ bond with respect to the bulk bond lengths of 2.45 Å. It is not established how the MEIS results would change if the fixed bond-length assumptions were relaxed. A second difference is found in the lateral displacement of the top layer which is related to the values of the shear angle and the bondlengths. Notwithstanding that the earlier LEED analysis by Meyer *et al.*³³ gives a better match to the MEIS simulations for the lateral displacements, the fully optimized geometry presented in Table I and the independent results of Puga *et al.*³⁴ each indicate a small difference be-

tween the LEED and MEIS, although this difference may lie within the intrinsic inaccuracies of the various models.

The previous LEED analyses^{22,33} using the Duke-Laramore-Beeby formulation differ from the present one in a variety of ways. In the previous studies the IV data was collected by an independent group using different ex-

perimental methods. Only 14 beams and a smaller energy range were analyzed. The previous theoretical model maintained a constant inelastic collision mean-free path, used phase shifts computed for ionic Ga^+ and As^- , and computed a surface slab of three bilayers exactly. An energy-dependent mean-free path, neutral atom phase

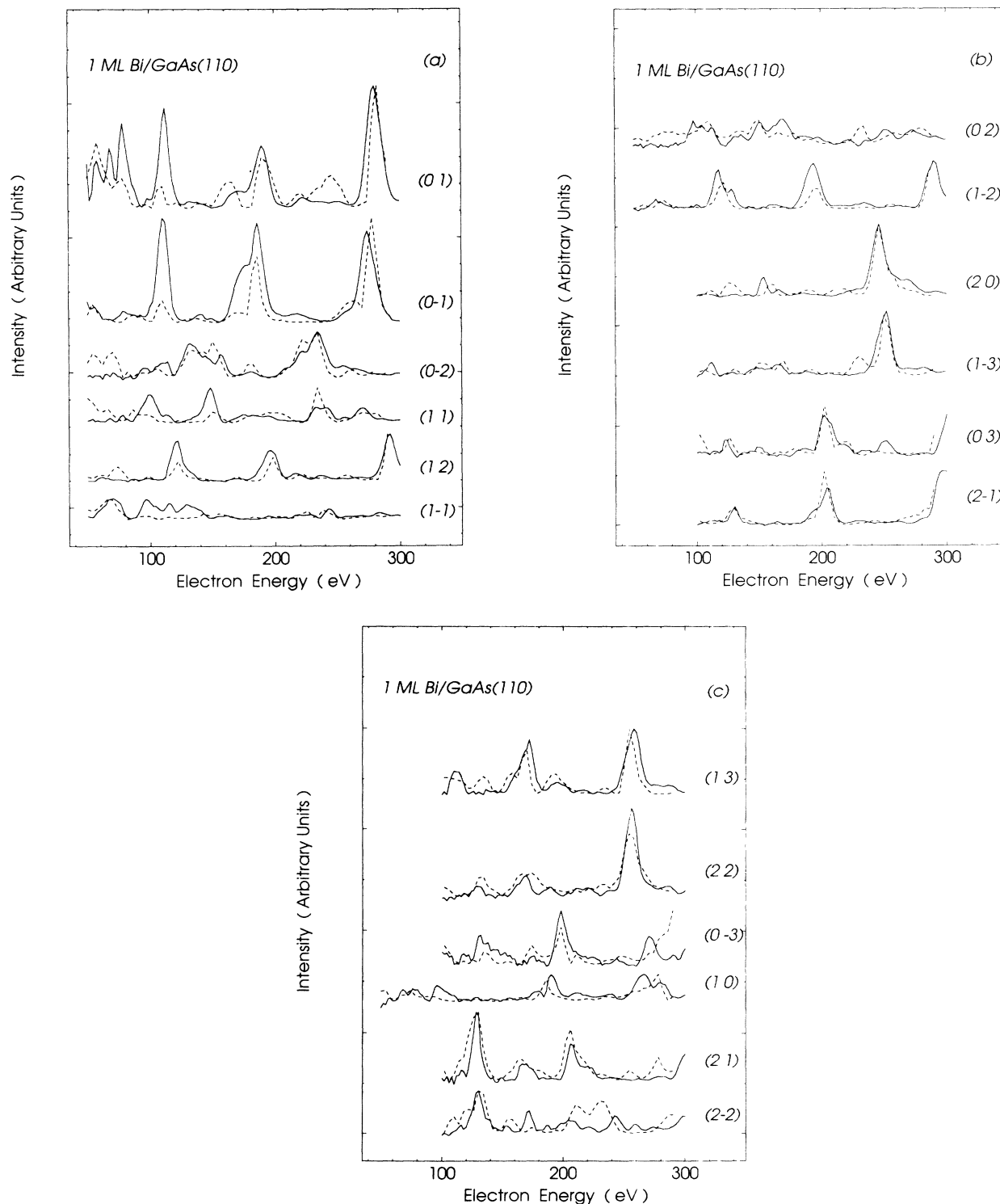


FIG. 9. Bi/GaAs(110) IV data, solid curves, grouped according to integrated beam intensities. The relative intensities of the beams are retained within each panel. The dashed lines are the computed intensities of the best fit structural model listed in Table I.

TABLE IV. Comparison of best fit Goddard geometries to previous work. See text for a description of the notations.

| GaAs(110) | ω_1 (deg) | $\Delta_{1,1}$ (Å) | ω_2 (deg) | $\Delta_{2,1}$ (Å) | $\delta y(\text{As})$ (Å) | $\delta y(\text{Ga})$ (Å) | $\delta d_{12,1}$ (Å) |
|----------------------------------|---------------------|-----------------------|---------------------|-----------------------|------------------------------|------------------------------|--------------------------|
| This work | -28.4 | 0.70 | 3.4 | 0.08 | 0.23 | 0.35 | -0.16 |
| Duke <i>et al.</i> ^a | -31.1 | 0.69 | 2.4 | 0.06 | 0.24 | 0.51 | -0.19 |
| Puga <i>et al.</i> ^b | -30.0 | 0.71 | 2.4 | 0.06 | 0.17 | 0.36 | -0.16 |
| Meyer <i>et al.</i> ^c | -27.3 | 0.65 | 4.9 | 0.12 | 0.33 | 0.49 | -0.18 |
| MEIS (Ref. 35) | -29.0 | 0.69 | 0.0 | 0.00 | 0.34 | 0.51 | -0.14 |

| Sb/GaAs(110) | ω_1 (deg) | $\Delta_{1,1}$ (Å) | ω_2 (deg) | $\Delta_{2,1}$ (Å) | $d_{12,1}$ (Å) | θ (deg) |
|--------------|---------------------|-----------------------|---------------------|-----------------------|-------------------|-------------------|
| This work | -2.3 | 0.08 | 4.5 | 0.11 | 2.34 | 92.4 |
| Ref. 2 | -2.9 | 0.10 | 4.0 | 0.10 | 2.39 | 91.1 |

| Bi/GaAs(110) | ω_1 (deg) | $\Delta_{1,1}$ (Å) | ω_2 (deg) | $\Delta_{2,1}$ (Å) | $d_{12,1}$ (Å) | θ (deg) |
|--------------|---------------------|-----------------------|---------------------|-----------------------|-------------------|-------------------|
| This work | -2.6 | 0.09 | 4.3 | 0.11 | 2.52 | 88.3 |
| Ref. 10 | -2.7 | 0.10 | 3.2 | 0.08 | 2.48 | 86.4 |

^aReference 22.^bReference 34.^cReference 33.

shifts, and a surface slab of four bilayers have been used here. Finally, our present structure search methodology represents a more thorough approach than has been used previously. Despite these differences in the theoretical models the structures derived are reassuringly similar, which helps substantiate the utility of LEED in surface atomic geometry calculations.

The disordered model for Sb and Bi overlayers on GaAs(110) is clearly ruled out on the basis of the LEED analysis given in Table II. The R_x factors listed in the table are too large to suggest a good fit. Furthermore, different initial starting points in the search led to different local minima. One expects this kind of ambiguity when the structural model is inconsistent with the IV data. Hence, the LEED analysis is compatible with the STM micrographs which depict an ordered overlayer for both the Bi and Sb systems.^{3,15}

The relaxed Skeath model failed to produce a satisfactory fit to the IV data for both Sb/GaAs(110) and Bi/GaAs(110). Several starting geometries were used, including ones with γ near 60° and others with γ near 90° , cf. Fig. 2. Searches using both fixed bond lengths and variable bond lengths were performed. In some cases, the value of γ moved toward 0° as a consequence of the simplex search. These cases were discarded as being unphysical because the corresponding nearest-neighbor distances were too small. One observes referring to Fig. 2 that for very large values of γ the Goddard geometry is recovered. This observation was tested for Sb/GaAs by varying γ from 40° to 275° , keeping β and ω at zero and the bond lengths at the covalent values. The result was an R_x curve that oscillated rapidly with increasing γ . The two deepest minima were near 60° and 230° , corresponding respectively to the Skeath and Goddard geometries. The best fit results where γ is constrained to lie between 20° and 180° are listed in Table III. However,

we observed that the results of the optimization depended on the choice of initial simplex. The sensitivity of the calculations to the initial starting geometry and the large R_x values computed cause us to reject this model as a possible geometry for either Sb/GaAs or Bi/GaAs.

It is interesting that for the Sb/GaAs(110) case our best fit Skeath geometry is close to that predicted from total energy minimization calculations.⁵ We believe this result is serendipitous because the multiple-scattering analysis is most sensitive to nearest neighbor distances. The presence of bonds and valence electron charge density is not included in the LEED calculations except in a very indirect manner via the self-energy term and the scattering phase shifts. A similar observation cannot be made for Bi/GaAs(110) where γ is near to 37° .

On the basis of our LEED analysis the Goddard model, cf. Fig. 1, is the most probable atomic geometry for Sb/GaAs(110) and Bi/GaAs(110). The results of our calculations for these two systems are listed in Table I and are compared to the literature in Table IV. Generally speaking, the geometry predicted on the basis of our simultaneous multidimensional search is indistinguishable from our earlier predictions. This observation is noteworthy for the Sb/GaAs(110) case where the experimental data were collected by a different group.² The quality of fit for the Sb/GaAs system, with $R_x = 0.199$, is better than that for Bi/GaAs, with $R_x = 0.238$. We believe that this may be a manifestation of the neglect of the sixth-order periodicity observed for the Bi/GaAs(110) system.¹¹ An exact (6×1) LEED calculation would have to be attempted to check this prediction.

By comparing the best fit results of the Sb and Bi systems we find corroboration of the concept of p^2 bonding within the overlayer. This model requires that the Sb—Sb—Sb or Bi—Bi—Bi bond angle θ be very close to 90° , which, in turn, requires modification of the corre-

sponding covalent bond lengths. Our best fit results indicate that the Sb—Sb and the Bi—Bi bond lengths undergo contractions relative to their covalent values by 1% and 2%, respectively, which is consistent with expectations based on the p^2 and s lone-pair bonding predicted for this geometry.^{2,6} The bond-length variation for the Sb/GaAs case produces an inconsequential 0.005 improvement in the R_x value and an increase in θ to 92° from the covalent bond-length value of 91°, cf. Table IV. For comparison, the tight-binding calculations which have, as yet, only been reported for Sb/GaAs predict a θ of 94°. The changes we report for Sb/GaAs are too small to be viewed as meaningful indicators. The changes for the Bi/GaAs case are, however, larger. Bond-length variations induce an improvement of 0.02 in R_x and an increase in θ to 88° from 86°, which taken together indicates a preference for the $90^\circ \pm 2^\circ$ structure and support of the p^2 model of bonding. We extend this inference to the Sb/GaAs system where the analysis is less conclusive. We also predict an expansion of the Sb—Ga and Bi—Ga bond lengths relative to their covalent values of 2% and 4%, which results because the covalent bond length is an unsuitable measure for an overlayer chain that is bonded to the substrate via hybridization of the Sb or Bi π band of states with the substrate sp^3 band. The predicted bond-length expansion is, therefore, a manifestation of the atomic size mismatch of the overlayer with the substrate.

The sensitivity of our LEED analysis technique to the choice of the physical model deserves some attention because the analysis utilizes multidimensional optimization. The optimization procedure, itself, has proven reproducible and independent of the starting conditions when applied to the Goddard model. It failed, however, in this regard when applied to the disordered and the relaxed Skeath models. We conclude that the occurrence of irreproducibility and starting condition dependence indicates the use of an incorrect structural model and is not an artifact of the multidimensional optimization method. The importance of the structural parameters in the analysis can be inferred by comparing Tables I and II. The results labeled 2 in Table II correspond to the rigid bond-length searches of Table I for Sb/GaAs and Bi/GaAs except that the Sb and Bi adatom scattering phase shifts were replaced by GaAs ones. Although the converged R_x geometries in Table II are similar to the corresponding ones given in Table I, the quality of fit is significantly worse than R_x values exceeding 0.3. This result serves to quantify the concept that multiple-scattering analyses are most sensitive to the physical geometry and secondary to the nonstructural aspects of the model, in this case the choice of atomic phase shifts.

VI. SYNOPSIS

Recent theoretical calculations have suggested that the accepted geometric model of Sb/GaAs(110), cf. Fig. 1, may be incorrect and that a different geometry, that of

Fig. 2, should be examined.⁵ In support of this observation scanning tunneling micrographs of the Sb/GaAs(110) system were shown to be consistent with both the geometry of Figs. 1 and 2.^{3,5} Furthermore, it was shown that the analysis of the angle-resolved photoemission measurements of surface-state bands for the Sb/GaAs(110) system could not distinguish between the two geometrical models.⁵ Finally, the previous LEED study of Sb/GaAs(110) did not conclusively rule out the alternate model because substrate relaxations were not included in the study.

Recent experimental studies have established that Bi and well as Sb forms epitaxial monolayers on GaAs(110).^{11–15} An initial LEED analysis suggested that the geometry is similar to that given in Fig. 1 but did not perform a comprehensive test of other candidate geometries.¹⁰ Furthermore, despite the isovalency of Sb and Bi, important differences in their growth characteristics on the III-V (110) family were discovered.⁷ These differences may be explained if a reliable understanding of the surface chemical bond for each system could be determined.

In response to these observations we have performed a comprehensive multiple-scattering analysis of the LEED intensities from Bi/GaAs(110), Sb/GaAs(110), and GaAs(110). For each system the data was measured similarly using identical experimental conditions and then analyzed using a common theoretical model. We established excellent agreement between our results for GaAs(110) and previous studies performed by several groups and, thereby, provided a benchmark of the reliability of our approach. Furthermore, several important extensions to the LEED analysis technique have been implemented, including a nonlocal multidimensional optimization procedure.

Our conclusion is that the most probable geometry for both Sb and Bi/GaAs(110) is that shown in Fig. 1. The relaxed Skeath geometry, Fig. 2, failed to provide an acceptable fit to the LEED IV data for either system, despite a wide range of structural parameters tested. Thus, we have established that the bonding of Bi on GaAs(110) should be identical to that of Sb and, specifically, that the p^2 bonded chain applies to both Bi and Sb overlayers. This is noteworthy because Bi is known to order differently on III-V (110) surfaces having larger unit cells, e.g., GaSb(110), InAs(110), and InSb(110).⁷ The chemical bonding of Bi to these other systems remains to be determined.

ACKNOWLEDGMENTS

This work was supported by a grant from the National Science Foundation, Grant No. DMR-8705879, by the John von Neumann Computer Center, and by the National Center for Supercomputing Applications. The Pacific Northwest Laboratory is operated by the Battelle Memorial Institute for the U.S. Department of Energy under contract No. DE-AC06-76RL1830.

- *Present address: Intel Corporation, 5200 NE Elam Young Parkway, M/S AL3-15, Hillsboro, OR 97124.
- †Present address: Gould AMI Semiconductors, Research and Development, 2300 Buckskin Rd., Pocatello, ID 83201.
- ¹C. A. Swarts, W. A. Goddard, and T. C. McGill, *J. Vac. Sci. Technol.* **17**, 982 (1982).
- ²C. B. Duke, A. Paton, W. K. Ford, A. Kahn, and J. Carelli, *Phys. Rev. B* **26**, 803 (1982).
- ³P. Mårtensson and R. M. Feenstra, *Phys. Rev. B* **39**, 7744 (1989).
- ⁴F. Schäffler, R. Ludeke, A. Taleb-Ibrahimi, G. Hughes, and D. Rieger, *Phys. Rev. B* **36**, 1328 (1987).
- ⁵J. P. LaFemina, C. B. Duke, and C. Mailhot, *J. Vac. Sci. Technol. B* **8**, 888 (1990).
- ⁶C. Mailhot, C. B. Duke, and D. J. Chadi, *Phys. Rev. B* **31**, 2213 (1985).
- ⁷W. K. Ford, T. Guo, S. L. Lantz, K. Wan, S.-L. Chang, C. B. Duke, and D. L. Lessor, *J. Vac. Sci. Technol. B* **8**, 940 (1990).
- ⁸S. L. Chang, T. Guo, W. K. Ford, A. Bowler, and E. S. Hood, in *Atomic Scale Structure of Interfaces*, edited by R. D. Bringans, R. M. Feenstra, and J. M. Gibson (MRS, Pittsburgh, 1990), pp. 45–50.
- ⁹T. Guo, K. J. Wan, and W. K. Ford, in Ref. 8, pp. 39–44.
- ¹⁰C. B. Duke, D. L. Lessor, T. Guo, and W. K. Ford, *J. Vac. Sci. Technol. A* **8**, 3412 (1990).
- ¹¹T. Guo, R. E. Atkinson, and W. K. Ford, *Phys. Rev. B* **41**, 5138 (1990).
- ¹²T. Guo, R. E. Atkinson, and W. K. Ford, in *Proceedings of the Industry-University Advanced Materials Conference II*, edited by R. W. Smith (Advanced Materials Institute, Denver, 1989).
- ¹³J. J. Joyce, J. Anderson, M. M. Nelson, C. Yu, and G. J. Lapeyre, *J. Vac. Sci. Technol. A* **7**, 850 (1989).
- ¹⁴J. J. Joyce, J. Anderson, M. M. Nelson, and G. J. Lapeyre, *Phys. Rev. B* **40**, 10412 (1989).
- ¹⁵A. B. McLean, R. M. Feenstra, A. Taleb-Ibrahimi, and R. Ludeke, *Phys. Rev. B* **39**, 12925 (1989).
- ¹⁶F. A. Cotton and G. Wilkinson, *Advanced Inorganic Chemistry*, 4th ed. (Wiley, New York, 1980).
- ¹⁷M. Hansen and K. Anderko, *Constitution of Binary Alloys*, (McGraw-Hill, New York, 1958).
- ¹⁸T. Guo, R. E. Atkinson, and W. K. Ford, *Rev. Sci. Instrum.* **61**, 968 (1990).
- ¹⁹C. B. Duke, in *Surface Properties of Electronic Materials*, edited by D. A. King and K. P. Woodruff (Elsevier, 1988), Chap. 3.
- ²⁰A. Kahn, *Surf. Sci. Rep.* **3**, 193 (1983).
- ²¹E. Zanazzi and F. Jona, *Surf. Sci.* **62**, 61 (1977).
- ²²C. B. Duke, S. L. Richardson, A. Paton, and A. Kahn, *Surf. Sci.* **127**, L135 (1983).
- ²³G. E. Laramore and C. B. Duke, *Phys. Rev. B* **2**, 4783 (1970).
- ²⁴J. L. Beeby, *J. Phys. C* **1**, 82 (1968).
- ²⁵C. B. Duke and C. W. Tucker, *Surf. Sci.* **15**, 231 (1969).
- ²⁶W. K. Ford, C. B. Duke, and A. Paton, *Surf. Sci.* **112**, 195 (1985).
- ²⁷R. J. Meyer, C. B. Duke, and A. Paton, *Surf. Sci.* **97**, 512 (1980).
- ²⁸J. Philip and J. Rundgren, in *Determination of Surface Structure by LEED*, edited by P. M. Marcus and F. Jona (Plenum, New York, 1984), p. 409.
- ²⁹W. H. Press, B. P. Flannery, S. A. Teukolsky, and W. T. Vetterling, *Numerical Recipes in C* (Cambridge University Press, Cambridge, 1988).
- ³⁰C. B. Duke and A. Paton, *Surf. Sci.* **164**, L797 (1985), and references therein.
- ³¹A. R. Lubinsky, C. B. Duke, B. W. Lee, and P. Mark, *Phys. Rev. Lett.* **36**, 1058 (1976).
- ³²C. B. Duke, A. R. Lubinsky, B. W. Lee, and P. Mark, *J. Vac. Sci. Technol.* **13**, 761 (1976).
- ³³R. J. Meyer, C. B. Duke, A. Paton, A. Kahn, E. So, J. L. Yeh, and P. Mark, *Phys. Rev. B* **19**, 5194 (1979).
- ³⁴M. W. Puga, G. Xu, and S. Y. Tong, *Surf. Sci.* **164**, L789 (1985).
- ³⁵L. Smit, T. E. Derry, and J. F. Van der Veen, *Surf. Sci.* **150**, 245 (1985).

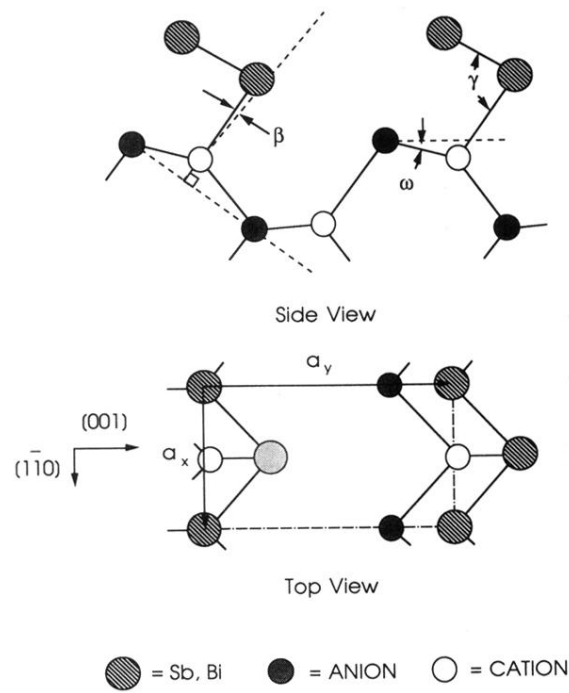


FIG. 2. Schematic drawing of the Skeath structural model depicting Sb or Bi bonded to a zinc-blende (110) substrate. β is positive, ω is negative, and $\gamma \approx \pi/2$, as depicted in the drawing.